# One-Pot Synthesis of Fe-N-Containing Carbon Aerogel for Oxygen Reduction Reaction

Youling Wang, Sandrine Berthon-Fabry

# One-pot synthesis of Fe-N-containing carbon aerogel for oxygen reduction reaction

Youling Wang [a], Sandrine Berthon-Fabry [a,*]

[a] MINES ParisTech, PSL University, PERSEE - Centre procédés, énergies renouvelables et systèmes énergétiques, CS 10207 rue Claude Daunesse 06904 Sophia Antipolis Cedex, France

*Corresponding author.

E-mail address: sandrine.berthon-fabry@mines-paristech.fr (S. Berthon-Fabry). Tel: +33 493957547. ORCID: 0000-0002-5281-3797

**Abstract**

Three-dimensional Fe-N-C aerogel catalysts for the oxygen reduction reaction (ORR) are prepared with resorcinol–formaldehyde–melamine and iron precursor using one pot sol-gel process followed by supercritical drying and heat treatment in nitrogen ($N_2$) and then ammonia ($NH_3$) atmospheres. We studied the effect of the synthesis conditions (Fe precursor and Fe content) of organic aerogel and the heat treatment parameters (including temperature and duration) under $N_2/NH_3$ atmosphere on the structural properties and ORR catalytic activities of the resulting Fe-N-C aerogel catalysts. The Fe-N-C aerogel catalysts were characterized by X-ray diffraction, scanning electron microscopy, X-ray photoelectron spectroscopy and $N_2$-adsorption/desorption, and the ORR activities were studied by the rotating disk electrode method. It was found that the pore structure, the chemical composition and ultimately the ORR performance were largely affected by the nature of iron precursor, iron content and the conditions of heat treatment. The catalysts using Iron (III) acetylacetonate as Fe precursor incorporated with 3 wt% of Fe followed by the HT at 800 °C for 1 h under $N_2$ and then 950 °C under $NH_3$ for 30 min, showed the highest content of active site (Fe-$N_x$) and largest mesopore volume, resulting in an enhanced catalytic activity and mass-transport property.

**Key words:** Non-precious metal catalyst, carbon aerogel, acidic media, oxygen reduction reaction

## 1. Introduction

The oxygen reduction reaction (ORR) is one of the most important reactions in energy storage/conversion systems such as PEM fuel cells (PEMFCs), Metal-air batteries etc. In PEMFCs, the kinetics of the ORR occurred at the cathode is found to be five times slower than the kinetics at the anode, leading to a high voltage loss through the system and as a result a diminished overall performance. To date, Pt-based catalysts are still considered as the most efficient catalysts for the ORR, whereas the high cost, scarcity and the poor durability of Pt hinder the practical application of PEMFCs [1]. Therefore, developing non-precious metal catalysts (NPMCs) for the ORR is of extreme significance and could be a long-term solution to realize the commercialization of PEMFCs. Among various NPMCs (e.g. transition metal oxides, carbides, nitrides, chalcogenides, metal-N-C catalysts, etc.), Fe-N-C materials have been regarded as the most promising alternative for the ORR in acidic medium [1–4]. In the past decade, much progress has been made in improving the activity and durability of the Fe-N-C catalysts and understanding the mechanisms in Fe-N-C-based ORR catalysis [1–4].

So far, there are mainly two ways to prepare Fe-N-C catalyst. The first method involves the incorporation of Fe and N into carbon (or N-doped carbon) materials (e.g. carbon black [5,6], carbon nanotubes [7,8], graphene [7], etc.) via pyrolyzing carbon material in the presence of nitrogen (e.g. melamine, polyaniline, polydopamine, etc.) and iron precursors at elevated temperatures under inert gas ($N_2$ or Ar) and/or active gas (e.g. $H_2$, $NH_3$) atmosphere. The other way is to directly pyrolyze the mixture of C, N and Fe precursors under inert and/or reactive gas atmosphere where heteroatom-doping and the formation graphitic carbon matrix occur at the same time [4]. To rationally design an efficient Fe-N-C catalyst, two factors should be taken into consideration. First, the intrinsic activity of the catalytic sites needs to be improved by adjusting the chemical composition of the catalysts and interactions between catalytic components. A consensus has been reached that micropore hosted Fe-$N_x$ sites exhibit the highest intrinsic ORR activity favoring the desirable 4-electron transfer [9–12]. Second, the accessibility to active sites should be maximized to facilitate rapid mass transport of ORR-related species ($O_2$, $H^+$, $H_2O$, etc.) within the catalyst layer, which is related to the quantity of meso/macro pores within catalysts [12]. Therefore, preparing Fe–N–C catalysts with a high density of Fe–$N_x$ moieties embedded in 3D carbon matrix comprising both micropores and larger pores (meso- or macrospores) could be a solution to combine the requirements for the high intrinsic activity and high accessibility to active sites.

Owing to the high surface area and pore volume, tunable pore size distribution, excellent electrical conductivity, carbon aerogels (CAs) have been considered as promising materials with a wide range of applications, including

supercapacitor [13,14], electro-sorption [15,16], metal air battery [17], and electrochemical reactions (e.g. ORR) in PEMFCs [18,19]. The highly porous structure and 3D interconnected network of aerogel-based catalyst allow an easier electrolyte access and better mass-transport capabilities. By incorporating N and Fe into carbon aerogels, 3D Fe,N-containing carbon aerogels could be a promising candidate for the ORR. These carbon aerogel-based catalysts are commonly prepared by sol–gel polycondensation of various organic monomers (such as resorcinol (R), melamine (M), phenol [20], formaldehyde (F) etc.) followed by heat treatment (HT) at elevated temperatures. Ave Sarapuu et al. prepared iron-containing nitrogen-doped CAs by pyrolysis of organic aerogels of variable composition from melamine, 5-methylresorcinol and 2,6-dihydroxy-4-methyl- benzoic acid where iron is introduced by ionic exchange on the surface of the gel. The ORR catalytic activity of the aerogel catalysts in alkaline electrolyte was found to increase with increasing the N and Fe content [21]. Liu et al. have integrated different transition metals (Fe, Co, Ni, Ti and Zr) into N-doped carbon xerogel prepared with resorcinol(R)-formaldehyde (F) resin as carbon precursor and $NH_3$ as nitrogen source in post heat treatment [22]. The results demonstrated that the metal had a great impact on both the ORR activity and physical properties of the resulting catalyst, and the iron-containing catalyst showed a better ORR activity. Furthermore, high-surface-area aerogel-like carbons were synthesized by Karina Elumeeva et al. based on carbonization of a specific ionic liquid (1-butyl-3-metyl-pyridinium dicyanamide, Bmp-dca) in the presence of transition metal (Fe or Fe/Co) precursors in salt melts [23]. The resulting catalysts exhibited high catalytic performance for the ORR in alkaline medium but a relatively low performance in acidic electrolyte. Compared with some ZIF-based Fe-N-C catalysts, the catalytic activities of reported carbon aerogels/xerogels were quite low especially in acid media [10,12,24]. It has been found that the structural characteristics, compositions and ORR catalytic activities of the resulting CAs are largely dependent on synthesis methods, choice of precursors (C, N and Fe precursors), synthesis conditions (pH, precursor composition) and HT protocols [22,23,25,26].

Different from previous studies, in this work, Fe-N-C aerogel catalysts were synthetized for the first time by one pot sol-gel polymerization process from resorcinol, melamine, formaldehyde and iron acetylacetonate (or iron acetate). The resulting gels were dried under supercritical condition followed by the pyrolysis in nitrogen ($N_2$) and then ammonia ($NH_3$) atmosphere. All the reactants are introduced in one pot, allowing a homogeneous distribution of carbon, nitrogen and iron in the bulk and on the surface, even in the micropores where Fe-$N_x$ active sites locate, ultimately achieving a promising ORR catalytic activity. The impact of iron content and the nature of iron precursor on the structure and catalytic performance in acid medium were investigated. Furthermore, the influences of the HT including the carbonization temperature in inert gas ($N_2$) and the duration of HT in $NH_3$ have also been studied. The pore structures and chemical

compositions of carbon aerogel catalysts were easily adjusted by varying the iron content and pyrolysis conditions, leading to an optimized mass-transport property and the highest intrinsic catalytic activity. In comparison to the reported aerogel-based Fe-N-C catalysts in the literature, the optimized catalysts in this work show a better catalytic activity in acid media in terms of onset potential, half-wave potential and mass activity [22,23].

## 2. Experimental

### 2.1. Sample synthesis

The Fe-containing hydrogels were prepared by a modified pre-polycondensation procedure using resorcinol (R), formaldehyde (F), melamine (M) and iron salt (Fe) as precursors, sodium carbonate (C) as catalyst and deionized water or ethanol as solvent (S) [15]. Fe-N-C aerogel catalysts with two different iron content, 1wt% and 3wt% were prepared using two different iron precursors (Iron (III) acetylacetonate-$Fe(acac)_3$ and Iron (II) acetate-$FeAc_2$) in order to study the impact of the nature of Fe precursor and Fe content on the resulting materials. The precursors were mixed at 70°C with the molar ratio of 2:7:1:0.033:60 for R:F:M:C:S. Subsequently, the pH of the mixture was adjusted to 8 by adding NaOH solution. Then, the gel was kept in water bath for 120 h at 70 °C for the aging process of the polymerized gel. Subsequently, the hydrogels were subjected to water-acetone exchange procedure before $CO_2$ supercritical drying. Afterward, the dried organic aerogel was carbonized at 800°C in $N_2$ for 1 h. Then, the carbonized sample was well ground, followed by a second pyrolysis at 950 °C under $NH_3$. For the denomination of the as prepared catalyst, the carbon aerogel catalysts with 1wt% of Fe using $FeAc_2$ as precursor heat-treated at 800 °C for 1h in $N_2$ and 950 °C in $NH_3$ for 30 min was denoted as CA-FeAc, 1wt%-800$N_2$-950$NH_3$. CA-Feacac, 3wt%-1050$N_2$-950$NH_3$-60min represents the carbon aerogel catalyst with 3wt% of Fe using $Fe(acac)_3$ as Fe precursor and heat-treated at 1050 °C for 1h in $N_2$ followed by a second HT at 950 °C in $NH_3$ for 60 min. For the purpose of comparison, Fe-free nitrogen-doped aerogel catalyst was also prepared under the same condition as Fe-containing catalysts just without the addition of Fe salt. Furthermore, the hydrogel presents an inconsistent texture due to the occurrence of sedimentation when 3wt% of Fe was incorporated using FeAc as iron precursor. Due to the inhomogeneity, all characterizations on this sample were discarded considering the unreliable reproducibility of the results.

### 2.2. Physicochemical characterization

Thermogravimetric analyses (TGA) were carried out by using a Labsys™ Evo TG instrument (Setaram, Caluire, France). The samples were heated at 10 °C $min^{-1}$ up to 1050 °C under an argon flow with a gas flow rate of 60 mL $min^{-1}$. The morphologies of the catalysts were investigated by scanning electron microscopy (SEM, ZEISS SUPRA™ 40)

operated at 3.0 kV. The surface area and pore characteristics of the catalysts were characterized by using nitrogen sorption isotherms at −196 °C with a Micromeritics ASAP 2020 instrument. Prior to the measurement, the samples were degassed under 10 mmHg at 200 °C for 496 minutes. The $N_2$-adsorption isotherms were used to determine specific surface area ($S_{BET}$), micropore volume ($V_\mu$), mesopore volume ($V_{meso}$), total pore volume ($V_T$) and pore size distribution (PSD). $S_{BET}$ was estimated using the Brunauer– Emmett–Teller (BET) equation. $V_T$ was determined from the adsorption volume at the relative pressure of 0.995. The $V_\mu$, $V_{meso}$ and micro-meso pore size distribution was calculated using the 2D-NLDFT-HS model assuming surface heterogeneity of carbon pores and pores with a slit geometry [27,28]. X-ray diffraction (XRD) analyses were performed using an X'pert Pro Philips diffractometer equipped with a Cu Kα source (λ = 0.15406 nm) operated at 45 kV and 30 mA. High score software was applied to determine the diffraction angles of the diffraction peaks under study. X-ray photoelectron spectroscopy (XPS) was used to identify the chemical state and determine the atomic concentration of chemical species in the samples. The measurements were performed using Thermo Scientific™ K-Alpha™ XPS spectrometer equipped with an Al Kα1,2 monochromatic source (1486.6 eV). All samples were analyzed with a spot size of 200 μm, and tests on four different spots of each sample were conducted to ensure the accuracy of the measurement. A survey spectrum and higher resolution (HR) multiplex scan spectra (C1s, O1s, N1s and Fe2p core levels) were obtained. Quantification of the elements was carried out with CasaXPS software (Casa Software Ltd.) by fitting the core level spectra after a Shirley background removal. All HR-spectra were fitted using a Gaussian/Lorentzian line shape. All spectra have been recalibrated with respect to the C 1s core level peak at 284.8 eV resulting from hydrocarbon contaminants at the surface.

### 2.3. Electrochemical characterization

All electrocatalytic tests were performed in three-electrode cell at room temperature using a rotating disk electrode (RDE, OrigaTrod) with a potentiostat/galvaniostat from Bio-Logic (HCP-803). Reversible hydrogen electrode (RHE) and graphite electrode were used as the reference electrode and the counter electrode, respectively. A RDE with a glassy carbon (GC, 0.196 $cm^2$) was used as the substrate of the working electrode. The catalyst ink was prepared by mixing 10 mg of ground catalyst, 95 μL of 5 wt% Nafion, 752 μL of ethanol and 46 μL of milliQ-grade $H_2O$ which was subject to agitation and sonication alternatively for a total of 1 h. 7 μL of catalysts suspension was dropped onto the GC electrode, resulting in a catalyst loading of 0.4 mg $cm^{-2}$.

All electrochemical tests were carried out in 0.05 M $H_2SO_4$ aqueous solution. Prior to each electrochemical test, the electrolyte solution was purged with $N_2$ (or $O_2$) for 30 min, and $N_2$ (or $O_2$) was kept burbling in the solution during measurement but in a slower rate to maintain the gas atmosphere. Cyclic voltammetry (CV) between 0 and 1.0 V vs. RHE

at 50 mV $s^{-1}$ was carried out in unstirred $N_2$-saturated solution until obtaining a reproducible signal. Linear scan voltammetry (LSV) was performed at 10 mV $s^{-1}$ in $O_2$-saturated electrolyte between 1.1 and 0 V vs. RHE under five different rotation rates (1600, 1225, 900, 625 and 400 rpm).

All obtained data was ohmic-drop (iR-drop) corrected, where ohmic-drop was defined by the solution resistance between the working electrode and the reference electrode. All LSV curves were corrected by subtracting the background current recorded in $N_2$-saturated electrolyte. The kinetic current density of catalysts controlled only by the ORR kinetics was calculated by the Koutecky-Levich (K-L) equation as follows:

$$\frac{1}{j_k} = \frac{1}{j_F} - \frac{1}{j_{lim}}$$

where $j_k, j_F \; and \; j_{lim}$ is the kinetic current density (in mA $cm^{-2}$), faradic current density (in mA $cm^{-2}$) and limiting current density (in mA $cm^{-2}$), respectively.

The mass activity (in A $g^{-1}$) is defined by the following equation:

$$j_M = -\frac{i_k}{m}$$

where $j_M > 0$ and m is the catalyst loading (0.4 mg $cm^{-2}$) on the GC. $j_M$ at 0.8 V recorded at 1600 rpm was reported and compared.

## 3. Results and discussion

Thermogravimetric analyses were carried out in argon (Ar) from room temperature to 1050 °C to study the impact of the nitrogen thermal treatment on the organic aerogels. The TG profiles are given in Fig. 1. Slight differences could be observed on the final weight of the sample according to the synthesis parameters and the iron content. No visible effect of the iron could be noticed. Indeed, the curves are similar and in accordance with those reported by Rasines [16] and Vesela [29] obtained on resorcinol-melamine-based carbon materials witout iron. TG could be divided in three main steps. Between 20 and 140 °C, the mass loss could be ascribed to the elimination of the water adsorbed on the surface and probably the desorption of light residual organic precursors such as formaldehyde (about 9 wt%). The second step, between 140 and 406 °C is attributed to the elimination of water adsorbed on the deepest pores of the aerogel and to the beginning of the pyrolysis with the release of the volatile components (such as $H_2O$, $NH_3$ and $CO_2$ [29]) due to the break of methyl, hydroxyl and amine groups from aromatic nuclei (about 25 wt%). The sharp peak observed by dTG at 330 °C is mainly correlated to the release of by-products from the decomposition of formaldehyde, melamine and ammonia [16]. The last step above 406 °C is carbonization due to the breaking of the C-H bonds with a release attributed to $H_2O$, $CO_2$ and $H_2$ (about 26 wt% and 32 wt% for the sample with the higher content in iron). The dTG showed the overlapping of

the step 2 and 3 which is in accordance with the attributed released gases [29]. Finally at 1050 °C the remaining mass is between 34 and 38 wt%. From the TG profiles, it could be noted that the mass loss above 800 °C is not pronounced, so all samples were firstly pyrolyzed at 800 °C in $N_2$ for 1h in order to carbonize organic aerogels. The effect of $NH_3$ treatment, Fe precursor and Fe content on the physiochemical properties and catalytic activities of as prepared aerogel catalysts were firstly studied.

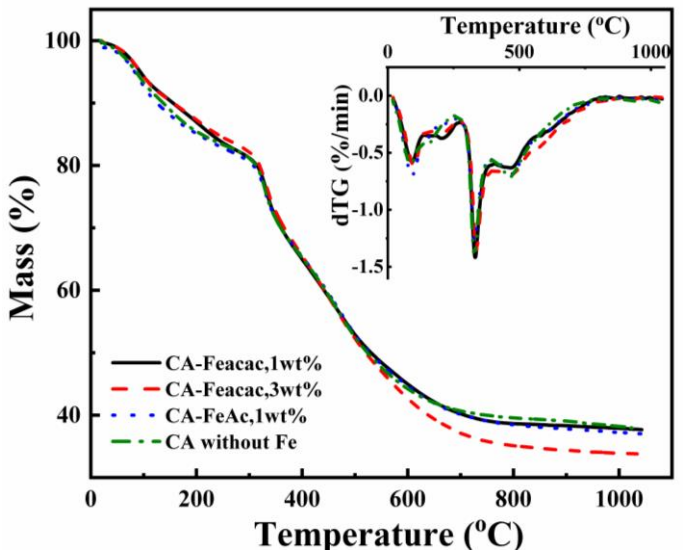


Fig. 1 Thermogravimetric (TG) and dTG (inset) profiles of the synthesized hydrogels.

Fig. 2 displays the SEM images of the catalysts obtained using two different Fe precursors with two different Fe content and the effect of the HT in $NH_3$ is shown. For comparison, the carbon aerogel without Fe is also presented. Without $NH_3$ treatment (Fig. 2a), the Fe-free catalyst exhibits a smooth and compact morphology. The catalysts containing 1wt% Fe (Fig. 2b and 2d) show a rough surface irrespective of the type of Fe precursor employed, whereas the catalysts with 3wt% Fe using Feacac as Fe precursor (Fig 2c) show a 3D porous morphology composed of interconnected spheroidal nanoparticles. After $NH_3$ treatment, some pinholes appear on the surface of Fe-free carbon aerogel (Fig. 2e) and the textures of catalysts containing Fe (Fig. 2f, 2g and 2h) become fine and more porous, which is due to the formation of micro- and mesopores during $NH_3$ treatment procedure. These SEM observations were in line with the results of $N_2$ sorption shown as follows.

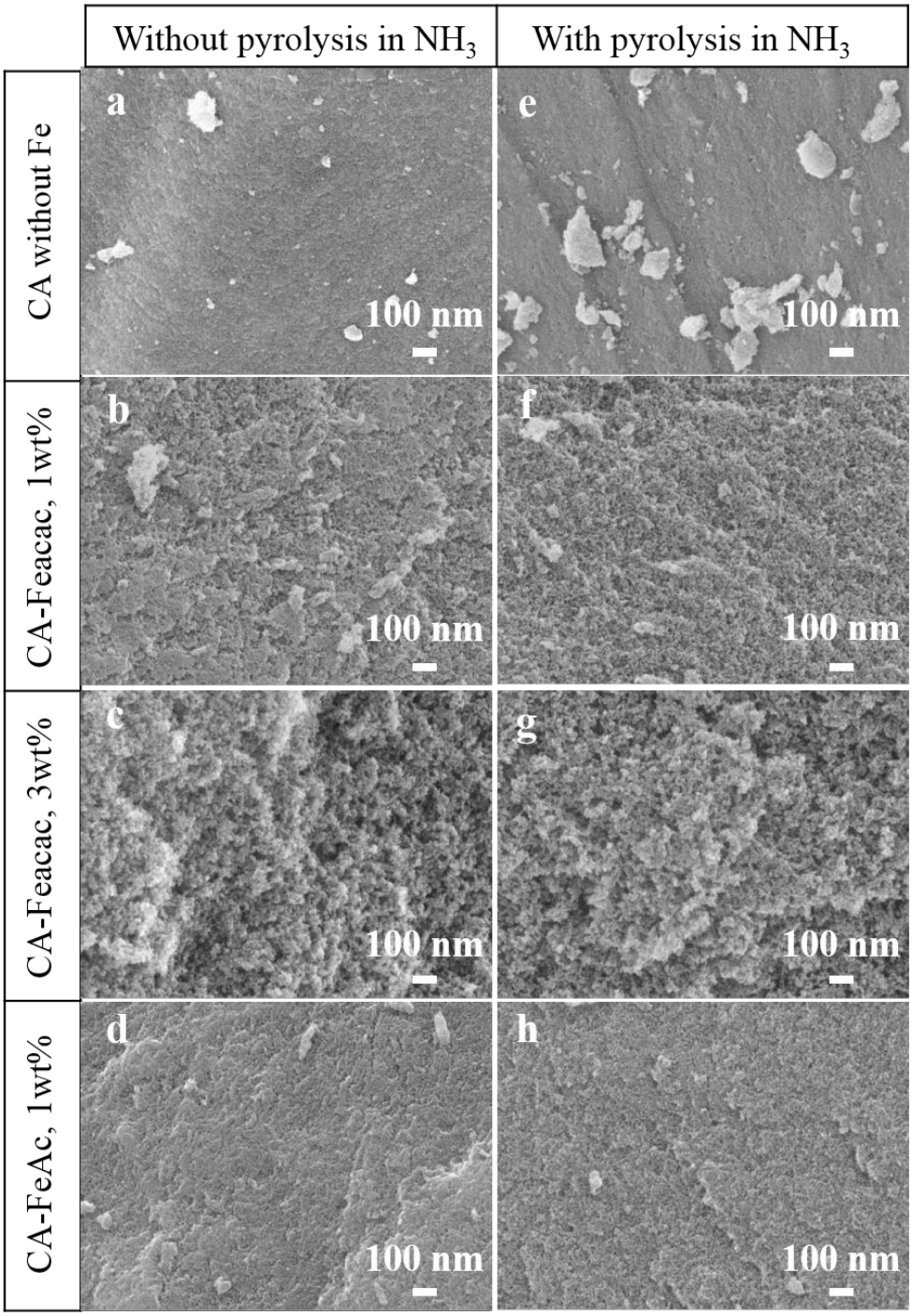


Fig. 2 SEM of catalysts with and without pyrolysis in $NH_3$ for carbon aerogels without Fe (a and e), with 1wt% of Fe using Feacac precursor (b and f), with 3wt% of Fe using Feacac precursor (c and g) and with 1wt% of Fe using FeAc precursor (d and h).

The textures of the as-prepared aerogels were characterized by $N_2$ sorption. Representative $N_2$ adsorption/desorption isotherms and PDS curves are shown in Fig. 3, and the relevant data is summarized in Table 1. Independent on Fe precursor used, Fe content and $NH_3$ treatment, all samples show a type IV isotherm, including features associated with micro/mesoporous materials. The isotherm presents a steep rise at low pressures, indicating the presence of micropores in large quantities, in particular for samples subjected to the $NH_3$ thermal treatment. At higher pressures, multilayer adsorption occurs, followed by pore condensation accompanied by a hysteresis loop. Catalyst with 3wt% Fe presents a H1 hysteresis loop associated with porous materials possessing a narrow distribution of relatively uniform

pores. In contrast, catalysts without Fe and containing 1wt% Fe for both Fe precursors show H2 hysteresis loops, indicative of interconnected networks of pores of different size and shape.

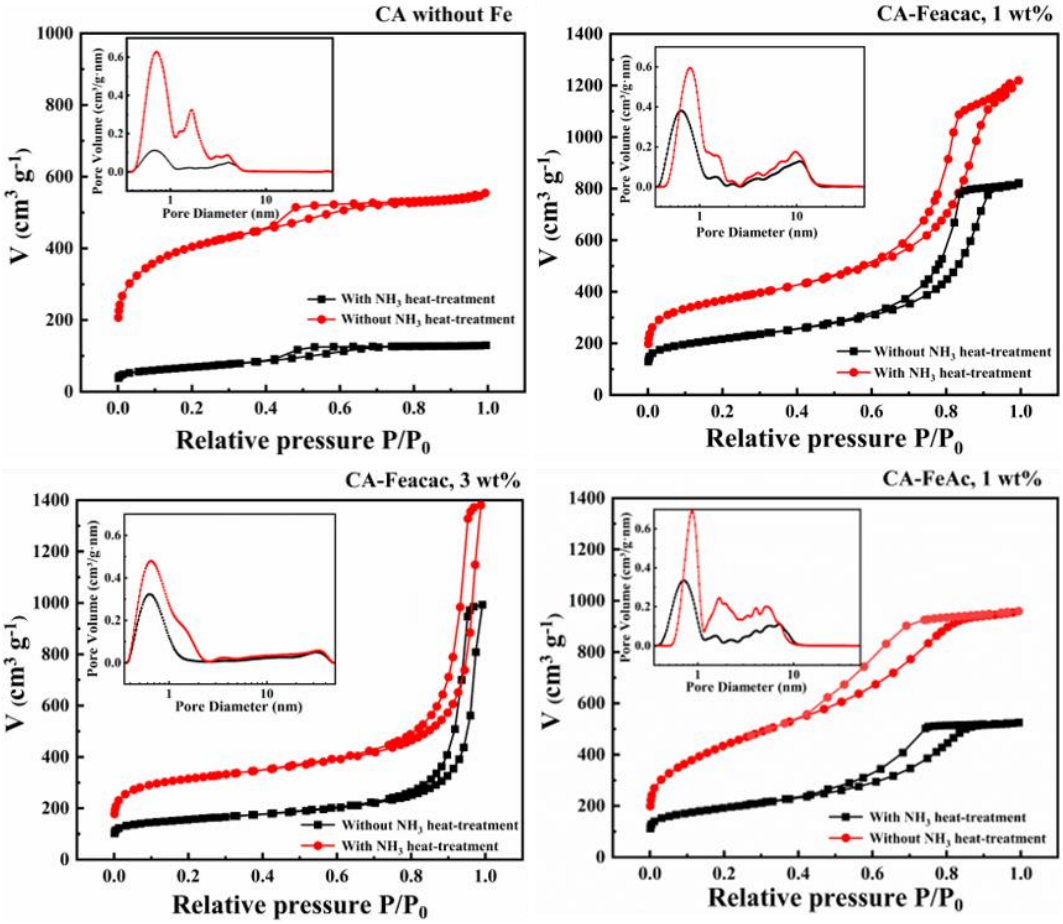


Fig. 3 $N_2$ adsorption isotherms at 77 K of the Fe-N-C aerogels pyrolyzed at 800 °C in $N_2$ with and without HT in $NH_3$. Inset: Pore size distribution plots obtained by using the 2D-NLDFT-HS method.

From Table 1, it can be noticed that the Fe content largely affects the porosity of the prepared materials. Remarkable difference in the total and mesopore volumes could be observed when the Fe content increase from 0 to 1wt % then to 3wt% event if the pH is maintained constant (pH=8). CAFeacac, 3wt% exhibits the highest meso-pore volume which could facilitate the mass transport of ORR-related species (e.g. $H^+$, $O_2$, $H_2O$ etc.) within the catalyst layer. Furthermore, regardless the iron precursor used the catalysts with a lower Fe content (1 wt%) exhibit a higher $S_{BET}$ which is mainly contributed by the higher micro-pore content as confirmed by the increase in the ratio of $V_{micro}/V_{meso}$ and is in line with their dense morphologies observed by SEM. This suggests that the addition of Fe could promote the formation of mesopores, leading to a higher total pore volume but a decreased $S_{BET}$. A similar phenomenon was also observed when carbon black additive was incorporated into carbon aerogel [30]. It was found that increasing the amount of carbon black led to a higher total pore volume and an enlargement of the average mesopore size. Furthermore, it can be also noted that BET surface area ($S_{BET}$) and pore volumes ($V_{T,\ micro\ and\ meso}$) of catalysts increase significantly after $NH_3$ treatment, compared with their counterparts pyrolyzed only in $N_2$. This significant increase in $S_{BET}$ and $V_{T,\ micro\ and\ meso}$ is due to the

formation of micropores and mesopores during HT in $NH_3$, which is proved by the increase in the value of micro-pore volume ($V_{micro}$) and meso-pore volume ($V_{meso}$), as well as verified by the PDS curves shown in the insets of Fig. 3. As can be seen, there is a large increase in the pore volume in the micro/meso pore region for the catalysts heat-treated in $NH_3$. The pore formation accompanied with mass loss during HT $NH_3$ is ascribed to the carbon gasification reaction composed of the main reaction ($C + NH_3 \rightarrow HCN + H_2$) and a minor reaction ($C + 2H_2 \rightarrow CH_4$) [31–33].

Table 1 Main textural parameters of the synthesized Fe-N-C aerogels derived from $N_2$ sorption

| Heat treatment | Iron precursor - Iron content (wt %) | $S_{BET}$ ($m^2\ g^{-1}$) | $V_T$ ($cm^3\ g^{-1}$) | $V_{micro}$ ($cm^3\ g^{-1}$) | $V_{meso}$ ($cm^3\ g^{-1}$) | $V_{micro}/V_{meso}$ |
|---|---|---|---|---|---|---|
| 800°C, $N_2$ Without HT in $NH_3$ | CA without Fe | 234 | 0.2 | 0.07 | 0.12 | 0.58 |
| | CA-Feacac,1wt% | 777 | 1.27 | 0.2 | 1.04 | 0.19 |
| | CA-Feacac,3 wt% | 572 | 1.54 | 0.17 | 1.29 | 0.13 |
| | CA-FeAc,1wt% | 682 | 0.81 | 0.18 | 0.6 | 0.30 |
| 800°C, $N_2$ With HT in $NH_3$ | CA without Fe | 1442 | 0.86 | 0.49 | 0.30 | 1.63 |
| | CA-Feacac,1wt% | 1332 | 1.89 | 0.37 | 1.46 | 0.25 |
| | CA-Feacac,3 wt% | 1164 | 2.14 | 0.37 | 1.69 | 0.21 |
| | CA-FeAc,1wt% | 1542 | 1.48 | 0.38 | 1.01 | 0.38 |

Fig. 4 shows the XRD patterns of the as-prepared catalysts. $N_2$-pyrolyzed catalysts present two broad peaks at around 25.5° and 44° assigned to (002) and (101) diffractions of carbon (JCPDS NO. 01-071-1621) with a low graphitic degree. From the enlarged view in the range of 35-55°, XRD profile of CA-Feacac, 3 wt%-800$N_2$ exhibit $Fe_3C$ peaks located at 37.6°, 42.8°, 45.8° and metallic Feα peaks at 44.7°, 65° and 82.3°. As the iron content decreases from 3wt% to 1wt%, the diffraction intensity of Feα decreases and $Fe_3C$ peaks become invisible. For catalysts containing 1wt% of Fe using FeAc as iron precursor, only a weak peak at 44.7° could be seen attributed to the (110) reflection of Feα. After the HT in $NH_3$, the intensity of C (002) peak at 26° increased, which could be resulted from the enhanced graphitization degree of carbon matrix at an elevated temperature of 950 °C and the gasification reaction of disordered carbon in catalysts with $NH_3$ [6,33,34]. Two peaks at 43.7° and 50.8° emerge for all the Fe-containing catalysts with the HT in $NH_3$, ascribed to (111), (002) planes of Fe nitride ($FeN_{0.0324}$, JCPDS NO. 01-075-2127) and/or Feγ (JCPDS NO. 99-900-8470) which is the phase appears above 910 °C based on the iron-carbon eutectic phase diagram. For Fe-free catalyst, only two broad peaks at around 25.5° and 44° indexed to carbon could be observed before or after the HT in $NH_3$. The graphitization degree of Fe-free catalyst under the same HT conditions is apparently different from Fe-containing catalysts. This is because Fe could promote the graphitization degree at elevated temperatures [35].

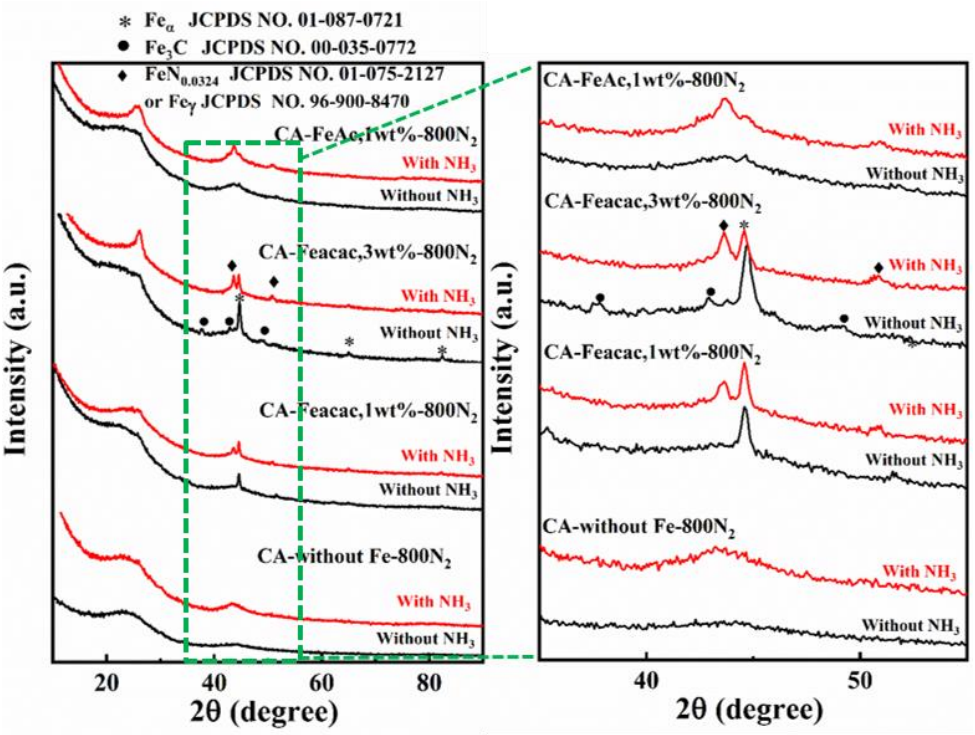


Fig. 4 XRD patterns (Left) and enlarged view (Right) of Fe-containing and Fe-free aerogel catalysts

The chemical composition at the surface of the catalysts was probed by X-ray photoelectron spectroscopy (XPS). The XPS survey spectra as shown in

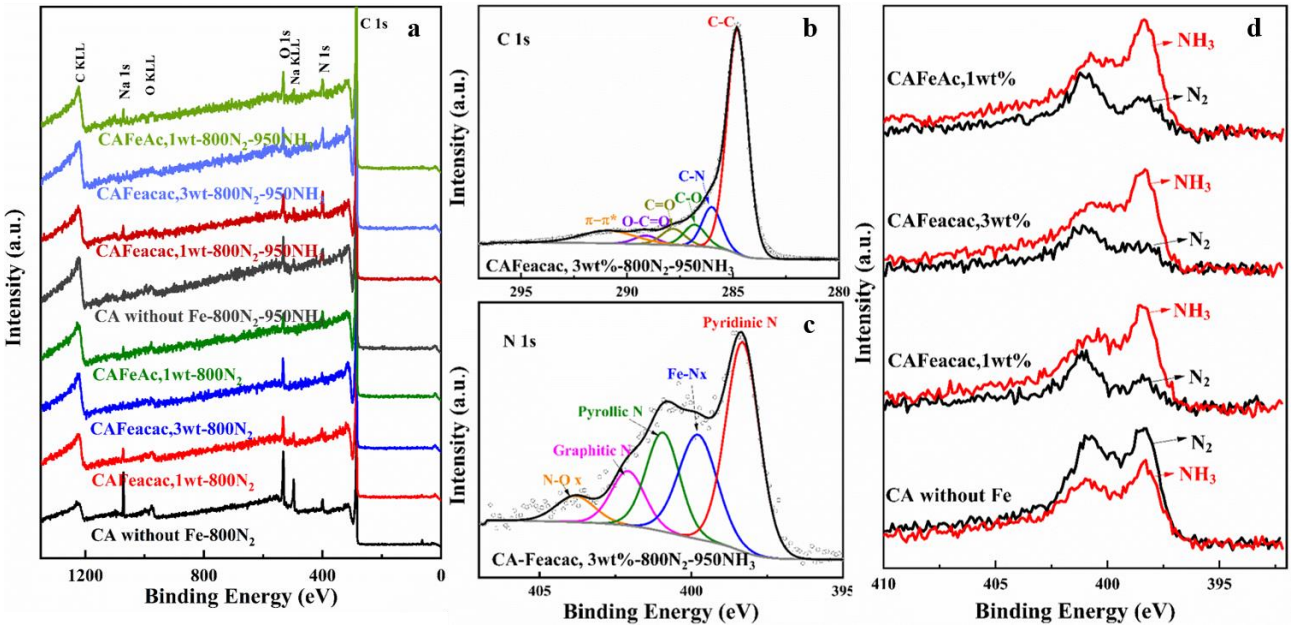


Fig. 5a reveal the signals of C, N, O, Na existing on the surface of all samples. The signal of Na is originated from the catalyst ($Na_2CO_3$) and NaOH used to adjust pH of initial solution during sol-gel process. As an example, all C 1s and N1s core-level spectra were deconvoluted as shown in

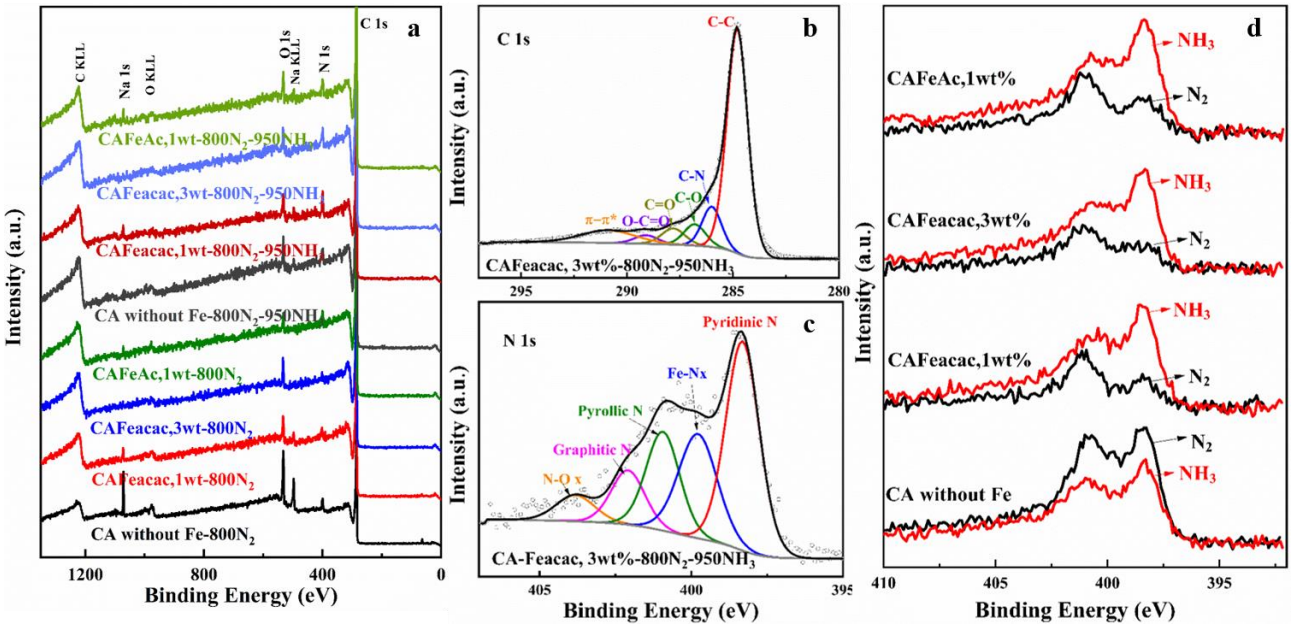


Fig. 5b and

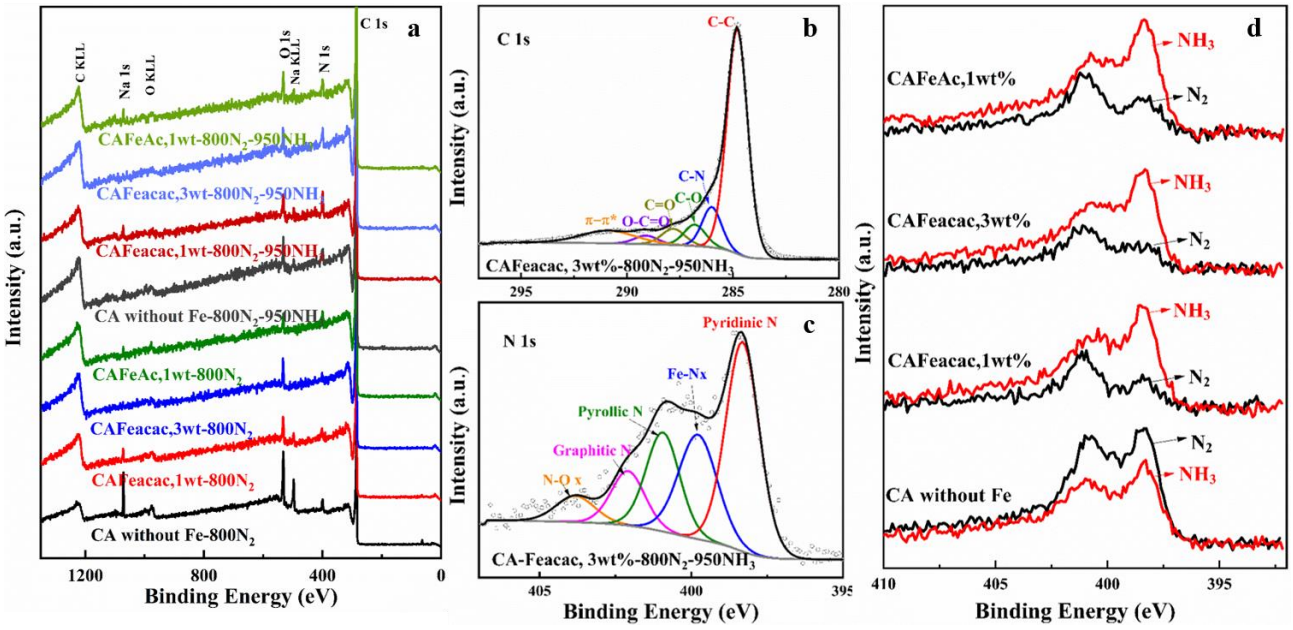


Fig. 5c, respectively. The C1s core-level spectra was deconvoluted into six peaks centered at 284.8, 286.0, 286.8 eV, 287.8, 289.1 and 290.7 eV, respectively assigned to different C functionalities from C-C, C-N defects, C-O, HO-C=O and π-π* [36]. The N1s core-level spectra (

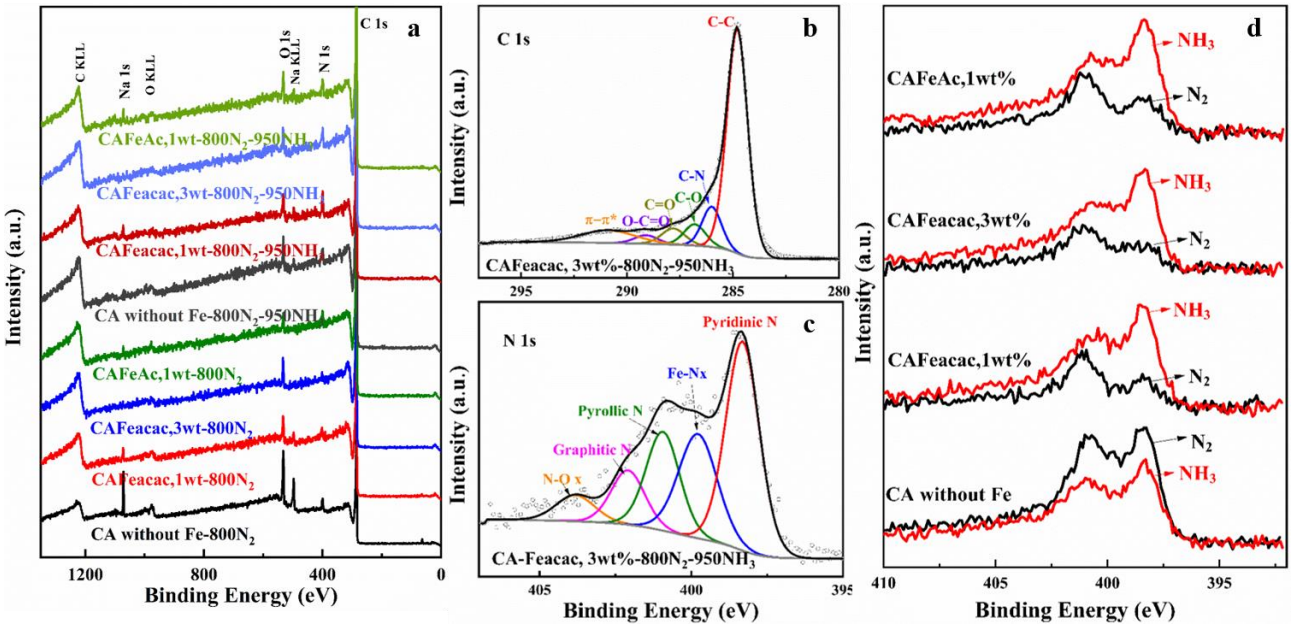


Fig. 5c) exhibit 5 characteristic peaks ascribed to pyridinic N (N-6), N coordinated to Fe (Fe-$N_x$, $x \leq 4$) for Fe-containing catalysts, pyrrolic N (N-5), graphitic and/or quaternary N (N-Q) and N-$O_x$ species at around 398.3, 399.4, 400.7, 401.9 and 404 eV, respectively [37,38]. The surface atomic composition and the relative content of different N species are summarized in Table 2. First, it could be noted that catalysts with HT in $NH_3$ show higher atomic N/C ratios. This is because that the HT in $NH_3$ increases the incorporation of N on the surface of the aerogel catalysts, which agrees with the observation in literature [33]. In addition, the HT in $NH_3$ also significantly influences the concentrations of different N species on the surface, especially for Fe-containing aerogel catalysts. As shown in Fig. 5d, pronounced evolution of N1s peaks could be seen when Fe-containing catalysts subjected to the HT in $NH_3$, displaying large increases in the range attributed to N-6 and Fe-$N_x$ along with the decrease in intensity ascribed to N-5, N-Q and N-$O_x$ contents. From the Table 2, it could be seen that the contents of N-6 and Fe-$N_x$ increase about 1.5 times after $NH_3$ treatment for all Fe-containing aerogel catalysts. It has been established that N-6 and Fe-$N_x$ largely contribute to the high catalytic activity of Fe-N-C catalysts [39,40]. By contrast, only minor change in N1s profile could be observed when Fe-free catalyst subjected to the same HT in $NH_3$. If comparing the N composition of catalysts prepared with different Fe precursor and different Fe content, no obvious distinction and trend could be noticed. These results reveal that the nature of Fe precursor and Fe content have less influence on the N composition of Fe-containing catalyst compared with the impact of thermal treatment in $NH_3$. Furthermore, no Fe 2p peak could be seen for both Fe-containing and Fe-free aerogel catalysts without $NH_3$ treatment. For Fe-containing catalysts, it is probably due to that Fe is encapsulated by graphitized carbon layers at elevated pyrolysis temperatures [38,39]. After $NH_3$ treatment, Fe 2p signals could be detected for Fe-containing catalysts. It was found that catalyst with a higher Fe loading (3 wt%) exhibits a higher Fe/N atomic ratio and higher Fe-$N_x$ content

after $NH_3$ treatment. It was reported that Fe content is a vital factor determining the ORR catalytic activity of Fe-N-C catalyst. Jiang et al. reported the ORR activity increased as the amount of Fe precursor was increased, because the presence of more crystalline Fe species was suggested to enhance the activity of the N and $FeN_x$ sites surrounding Fe nanoparticles [41]. Xu et al. found that the Fe and Co salts introduced a higher content of pyridinic N and $Me{-}N_x$ species, resulting in a better activity compared to catalysts prepared from other transition metals or those prepared without the addition of a metal [42].

Table 2 Surface Fe, N, and C atomic ratios and percentage of different N-species obtained by XPS.

| Heat treatment | Iron precursor - Iron content (wt %) | Fe/C | N/C | O/C | Fe/N | N-6 | Fe-$N_x$ | N-5 | N-Q | N-$O_x$ |
|---|---|---|---|---|---|---|---|---|---|---|
| 800°C, $N_2$ Without HT in $NH_3$ | CA without Fe | - | 0.049 | 0.141 | - | 45.52 | - | 29.22 | 17.14 | 8.12 |
| | CA-Feacac,1wt% | - | 0.015 | 0.028 | - | 26.87 | 12.93 | 37.63 | 15.15 | 7.42 |
| | CA-Feacac,3 wt% | - | 0.015 | 0.028 | - | 25.13 | 11.17 | 41.92 | 13.95 | 7.83 |
| | CA-FeAc,1wt% | - | 0.014 | 0.078 | - | 23.35 | 17.53 | 35.60 | 16.01 | 7.52 |
| 800°C, $N_2$ With HT in $NH_3$ | CA without Fe | - | 0.029 | 0.031 | - | 45.78 | - | 36.22 | 12.78 | 5.23 |
| | CA-Feacac,1wt% | 0.0006 | 0.039 | 0.028 | 0.015 | 40.15 | 23.06 | 21.05 | 9.80 | 5.95 |
| | CA-Feacac,3 wt% | 0.0007 | 0.028 | 0.025 | 0.028 | 40.59 | 23.5 | 20.69 | 9.57 | 5.66 |
| | CA-FeAc,1wt% | 0.0008 | 0.031 | 0.031 | 0.026 | 42.74 | 25.38 | 18.45 | 8.88 | 4.55 |

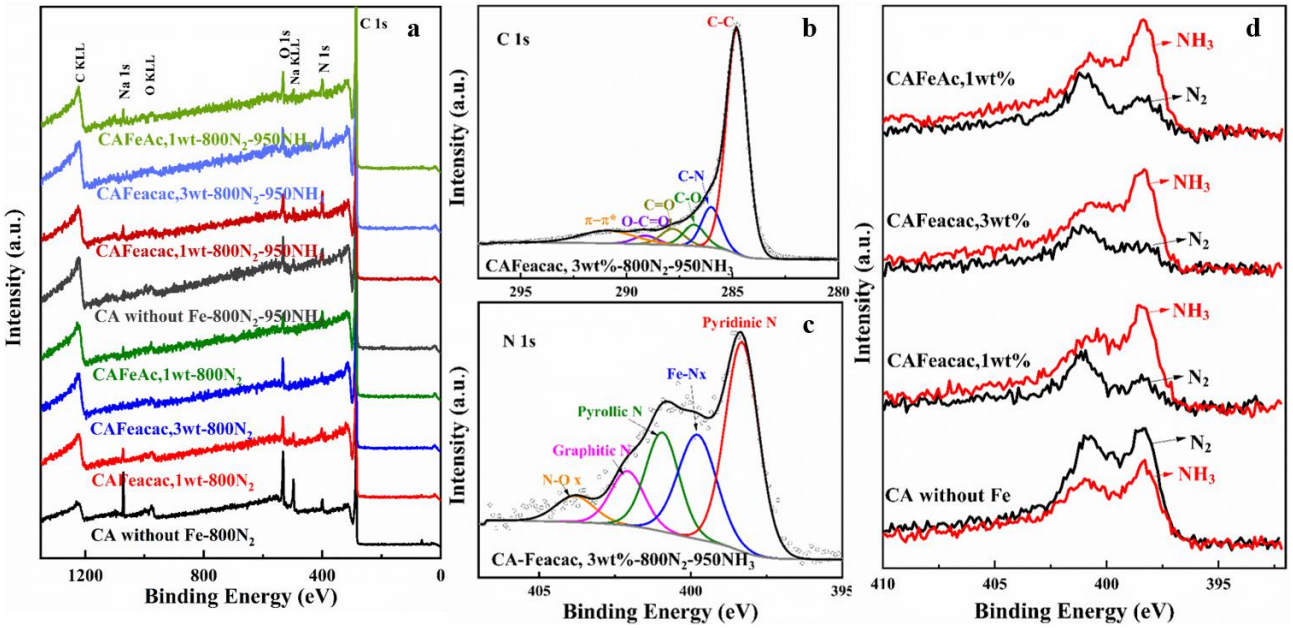


Fig. 5 XPS spectra and analyses of aerogel catalyst. Survey scans (a); High-resolution (HR) XPS spectra of C1s (b) and N 1s (c) for CAFeacac, 3wt%-800$N_2$-950$NH_3$; The comparison of N 1s (d) spectra prepared under different conditions.

On the basis of the physico-chemical characterizations of as-synthesized aerogel catalysts, the catalysts subjected to the second HT under $NH_3$ clearly display more interesting features for the ORR, including higher specific surface area, higher surface N and Fe contents and higher pyridinic N and Fe-$N_x$ catalytic sites. According to the literature, these characteristics are essential to obtain a higher ORR performance [1,12]. Therefore, the ORR performance evaluations by RDE were conducted on the catalysts with the HT in $NH_3$.

Fig. 6a presents the cyclic voltammograms (CVs) of catalysts subjected to HT in $NH_3$ recorded in $N_2$-saturated 0.05 M $H_2SO_4$ aqueous solution. All the CVs exhibit a rectangle profile which is typical characteristic of carbonaceous materials. The area-specific capacitance (the capacitance normalized by the specific surface area $S_{BET}$) reflects the magnitude of electrochemical surface area accessible to electrochemical reactions which is largely dependent on the specific surface area ($S_{BET}$) and the pore structure of catalysts [43]. The area-specific capacitances are 0.21, 0.24, 0.17 and 0.19 F $cm^{-2}$ for CAFeacac,1wt%-800$N_2$-950$NH_3$, CAFeacac,3wt%-800$N_2$-950$NH_3$, CAFeAc,1wt%-800$N_2$-950$NH_3$ and Fe-free catalysts, respectively. The higher area-specific capacitance of CAFeacac,3wt%-800$N_2$-950$NH_3$ is attributed to its higher pore volume particularly the higher meso-pore volume which allows a better accessibility to the surface of catalyst and could largely enhance the mass-transport properties of catalysts for the ORR. Fig. 6b compares the polarization curves of the catalysts. First, substantial improvement in ORR performance of catalysts containing metal in comparison with metal-free is observed, in terms of onset potential, half-wave potential and current densities within the whole potential range. The better ORR performance of Fe-containing catalyst is mainly due to the presence of Fe-$N_x$ active sites. By contrast, Fe-free catalysts contain only C-$N_x$ active sites which is less active than Fe-$N_x$ for the ORR. Among the Fe-containing catalysts, CAFeacac, 3wt%-800$N_2$-950$NH_3$ demonstrates the most positive onset potential of 0.845 V, the most positive half-wave potential of 0.72 V and the largest diffusion limiting current density compared to the catalysts with a lower Fe content of 1wt%. Furthermore, it also exhibits the highest mass activity ($j_k$) of 1.38 A $g^{-1}$ at 0.8 V vs. RHE, higher than CAFeacac, 1wt%-800$N_2$-950$NH_3$, CAFeAc, 1wt%-800$N_2$-950$NH_3$ and Fe-free aerogel with $j_k$ of 0.88, 1.18 and 0.41 A $g^{-1}$, respectively. Compared with some reported aerogel-based ORR catalysts tested in acidic medium, the ionic-liquid-derived carbon aerogel catalysts (NCA_CZ_Fe) showed a half-wave potential of 0.603 V which is lower than our best CA catalyst CAFeacac, 3wt%-800$N_2$-950$NH_3$ with a higher half wave potential of 0.72V [23]. In comparison to nitrogen-doped carbon xerogel doped with Fe (Fe-NCX), our best catalyst shows a more positive onset potential of 0.845 V and a higher mass activity of 20.6 A $g^{-1}$ at 0.7 V compared to 0.823 V and 8.6 A $g^{-1}$ (3.257 mA $cm^{-2}$ divided by 0.38 mg $cm^{-2}$) for Fe-NCX, respectively [22]. Fig. 6c displays the Tafel plots of all the catalysts. The initial Tafel slopes of Fe-containing catalysts are in the range of 64-66 mV $dec^{-1}$ close to the reported Fe-N-C catalysts in the literature and are apparently lower than that of Fe-free catalyst (81 mV $dec^{-1}$) [44]. The lower initial Tafel slope indicate a higher kinetics of Fe-containing catalysts for the ORR in comparison to Fe-Free catalysts. This is due to that the Fe-$N_x$ active sites in Fe-containing catalysts are more efficient for the ORR than C-$N_x$ sites on Fe-free catalysts. The electron-transfer number (n) of the catalysts over the potential range of 0.05-0.5 V were further studied by RDE analysis, as shown in Fig. 6d. The n values of CAFeacac, 3wt%-800$N_2$-950$NH_3$ in in the range of 3.77-4.01, which is close to the theoretical value of 4, indicating that the ORR occurs mainly through a 4-electron transfer. The observed enhancement in ORR

activity of CAFeacac, 3wt%-800$N_2$-950$NH_3$ could be correlated to its higher Fe-$N_x$ content and Fe/N atomic ratio on the surface. $FeN_x$ ensembles have been proven to be the most active sites for the ORR. Furthermore, it possesses a suitable pore structure for the ORR containing adequate micro-pores to accommodate Fe-$N_x$ sites and high mesopore volume up to 1.69 $cm^3$ $g^{-1}$ largely promoting the mass-transport properties of catalysts layer as demonstrated by the sharp transition region of kinetic-to-diffusion control in polarization curve and flat limiting current plateau.

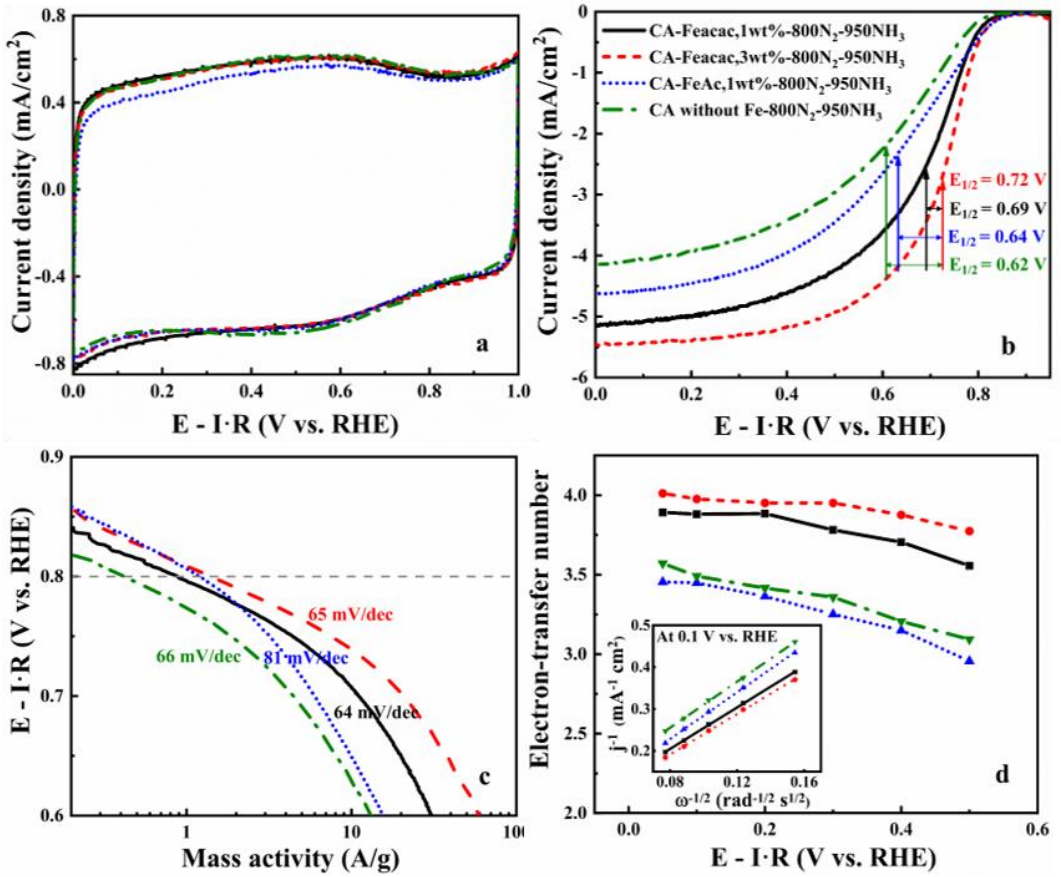


Fig. 6 CVs in 0.05 M $H_2SO_4$ deaerated solution with a potential scan rate of 10 mV $s^{-1}$ (a), polarization curves in RDE at 1600 rpm at 10 mV $s^{-1}$ $O_2$-saturated 0.05 M $H_2SO_4$ (b), tafel plots (c) and Electron-transfer number (d) over 0.05-0.7 V of catalysts. Inset of Fig. 6d: The K-L plot at 0.1 V vs. RHE.

According to the study of the impact of Fe precursor and Fe content, we could conclude that the best aerogel catalyst under study was obtained using Feacac as Fe precursor incorporated with 3wt% of Fe followed by the HT under $N_2$ and then $NH_3$. It is well known that HT parameters largely influence the catalytic activity of the resulting catalyst, including the HT temperature and duration in $N_2$ and $NH_3$ atmosphere [4]. Therefore, a further optimization on the HT parameters was conducted on CAFeacac-3wt% catalyst. First, the effect of carbonization temperature in $N_2$ has been studied. Organic aerogels were pyrolyzed at two different temperatures (800 and 1050 °C) for the same duration of 1h, followed by a HT at 950 °C in $NH_3$ for 30 min. The important characteristics for ORR catalysts including pore texture, chemical composition and ORR performance were studied by $N_2$ sorption, XPS and RDE techniques, respectively. The

corresponding information is presented in Table 3. For both carbonization temperatures at 800 °C and 1050 °C, certain weight losses could be observed during the pyrolysis in $NH_3$, accompanied with the enhancement in $S_{BET}$, pore volume (total, micro- and meso-pore) and surface N content and particularly the content of Fe-$N_x$, and as a result a higher mass activity compared with the catalysts pyrolyzed exclusively in $N_2$. As for the effect of carbonization temperature, CAFeacac-3wt%-800$N_2$-950$NH_3$ exhibits a better ORR activity in terms of mass activity and half-wave potential compared to the catalyst carbonized at 1050 °C followed by the same pyrolysis procedure in $NH_3$. High carbonization temperature at 1050 °C in $N_2$ causes the collapse of pore networks within aerogel [45], and the decomposition of N-C, N-Fe bonds on catalyst surface. This could be verified by the increase in the specific surface area surface and N (total N and Fe-$N_x$) content of the catalysts carbonized at the lower temperature of 800 °C then subjected to HT in $NH_3$. Furthermore, it could be noticed that the weight loss during the pyrolysis in $NH_3$ is lower, when the catalyst was initially carbonized at a higher temperature. With the same pyrolysis time of 30 min in $NH_3$, the weight losses were 32% and 9.7% for catalysts initially carbonized at 800 °C and 1050 °C. respectively. This is mainly due to that a higher initial pyrolysis temperature in $N_2$ leads to a higher graphitization degree, which could be verified by their TEM images (shown in Fig. S1 in the support information). As can be seen from the TEM images, the catalyst subjected to the HT at 1050 °C shows the interconnect grains part of which are apparently crystallized. The higher graphitization degree decreases the reaction rate between carbon matrix and $NH_3$, leading to a lower weight loss. According to the study of Jean-pol Dodelet's group, there is a direct correlation between the N content and the weight loss of the carbon matrix during the pyrolysis under $NH_3$ atmosphere [46]. $NH_3$ reacts with the disorganized carbon, fixing nitrogen atoms at the surface of the carbon matrix. The higher initially carbonization temperature at 1050 °C leads to a lower mass loss during the pyrolysis in $NH_3$, resulting in lower nitrogen atoms fixed on the catalyst surface and eventually a lower N content demonstrated by XPS measurement. To verify the weight loss effect, we have extended the duration of $NH_3$ treatment to 1 h and a weight loss of 32% was obtained for the catalyst initially pyrolyzed at 1050 °C in $N_2$. The increase in the HT time in $NH_3$ generates a higher weight loss along with enhancements in $S_{BET}$, pore volume (total, micro- and meso-pore) and surface N content and the content of Fe-$N_x$, leading to a higher mass activity and half-wave potential compared with that initially carbonized at the same temperature in $N_2$ but with a shorter duration of 30 min in $NH_3$. Based on the optimization study of HT conditions, it was found that the best HT protocol for CAFeacac, 3wt% catalyst is carbonization at 800°C for 1h followed by the second HT under $NH_3$ at 950 °C for 30 min. Even though the optimized catalytic activity of our new aerogel catalyst is still inferior to the performance of some catalysts reported in the literature (with some of them investigated for a long time), it is worth mentioning that most of better performed catalysts to date were synthesized from expensive precursors such as Zn(II) zeolitic imidazolate framework of formula $ZnN_4C_8H_{12}$ (ZIF-8) [10,12,24]. For this work, big progress in

catalytic performance for the ORR could be achieved by further adjusting other parameters of the synthesis process such pH, the solid content and so on. Therefore, the work present here could be a good start point for the study of carbon aerogel catalyst based on cheap precursors (R, F and M) and deserves further studies from both the fundamental and practical point of view.

Table 3 The information of CAFeacac, 3wt% catalyst under different pyrolysis conditions.

| Temperature in $N_2$ (°C ) | 800 | 800 | 1050 | 1050 | 1050 |
|---|---|---|---|---|---|
| Duration in $NH_3$ (min) | 0 | 30 | 0 | 30 | 60 |
| Weight loss in $NH_3$ | - | 32% | - | 9.70% | 32% |
| $j_k$ at 0.8 V vs. RHE (A/g) | - | 1.38 | - | 0.4 | 0.69 |
| $E_{1/2}$ (V) | 0.49 | 0.72 | 0.47 | 0.62 | 0.67 |
| Fe/C (at%/at%) | - | 0.0007 | - | 0.0002 | 0.0007 |
| N/C (at%/at%) | 0.0147 | 0.028 | 0.009 | 0.018 | 0.0185 |
| O/C (at%/at%) | 0.028 | 0.025 | 0.023 | 0.021 | 0.033 |
| Fe/N (at%/at%) | - | 0.025 | - | 0.011 | 0.040 |
| Pyridinic N (N-6) | 25.1 | 40.6 | 11.50 | 31.1 | 35.25 |
| Fe-$N_x$ | 11.2 | 23.5 | 9.01 | 21.34 | 21.24 |
| Pyrrolic N (N-5) | 41.9 | 20.7 | 38.78 | 24.17 | 24.73 |
| Quaternary N (N-Q) | 14.0 | 9.6 | 28.72 | 15.43 | 13.05 |
| Oxidized N | 7.8 | 5.6 | 12.00 | 7.98 | 5.73 |
| $S_{BET}$ ($m^2$ $g^{-1}$) | 572 | 1164 | 401 | 697 | 1023 |
| $V_T$ ($cm^3$ $g^{-1}$) | 1.54 | 2.14 | 1.37 | 1.82 | 1.96 |
| $V_{micro}$ ($cm^3$ $g^{-1}$) | 0.17 | 0.37 | 0.11 | 0.21 | 0.33 |
| $V_{meso}$ ($cm^3$ $g^{-1}$) | 1.29 | 1.69 | 1.16 | 1.52 | 1.56 |
| $V_{micro}/V_{meso}$ | 0.13 | 0.21 | 0.1 | 0.14 | 0.21 |

## 4. Conclusion

Fe-N-C aerogel catalysts have been prepared by one-pot sol gel polymerization of resorcinol, melamine, formaldehyde and Fe precursors ($Fe(acac)_3$ or $Fe(Ac)_2$), followed by supercritical drying and HT in $N_2$ and $NH_3$ gas flow at elevated temperatures. The impact of Fe precursor, Fe content and the HT conditions on the physicochemical properties and ORR catalytic activity of the as-synthesized catalysts have been studied. It was found that the impact of $NH_3$ is more significant than the nature of Fe precursor and Fe content, affecting several important properties such as the relative surface abundance of the Fe species, the surface N content, and electrochemically accessible surface area, all of which contribute to an increased catalyst activity. Nevertheless, the nature of Fe precursors and Fe content mainly affect the pore structure and has less impact on the composition of catalysts. Furthermore, the HT parameters were further optimized

as a function of mass loss during the HT under $NH_3$. It was found that a higher carbonization temperature leads to the partial collapse of pore network and the decomposition of active N species, resulting in a lower catalytic activity associated with the lower surface area, N surface content and Fe-$N_x$ content. As a result, the carbon aerogel catalysts incorporated with 3wt% of Fe using Feacac as Fe precursor followed by the HT at 800 °C for 1 h under $N_2$ and then 950 °C under $NH_3$ for 30 min, showed the highest catalytic activity in terms of onset potential and mass activity and the best mass transport properties.

**Acknowledgements**

The authors wish to thank Pierre Ilbizian for help with supercritical drying, Suzanne Jacomet for SEM analysis, Gabriel Monge for XRD and Frédéric Georgi for XPS (CEMEF- MINES ParisTech), Sergio Rojas for TEM analysis (CSIC Madrid), and the European Union's H2020-JTI-FCH-2017 Programme (number 779550, project PEGASUS) for funding this work.

## References

1. M. Shao, Q. Chang, J. P. Dodelet, R. Chenitz, Recent Advances in Electrocatalysts for Oxygen Reduction Reaction. Chem. Rev. **116**(6), 3594–3657 (2016).

2. L. Zhang, D. P. Wilkinson, Y. Liu, J. Zhang, Progress in nanostructured (Fe or Co)/N/C non-noble metal electrocatalysts for fuel cell oxygen reduction reaction. Electrochim. Acta **262**, 326–336 (2018).

3. H. Shen, T. Thomas, S. A. Rasaki, A. Saad, C. Hu, J. Wang, M. Yang, Oxygen Reduction Reactions of Fe-N-C Catalysts: Current Status and the Way Forward. Electrochem. Energy Rev. **2**(2), 252–276 (2019).

4. F. Jaouen, E. Proietti, M. Lefèvre, R. Chenitz, J. P. Dodelet, G. Wu, H. T. Chung, C. M. Johnston, P. Zelenay, Recent advances in non-precious metal catalysis for oxygen-reduction reaction in polymer electrolyte fuel cells. Energy Environ. Sci. **4**(1), 114–130 (2011).

5. S. Ruggeri, J. P. Dodelet, Influence of structural properties of pristine carbon blacks on activity of Fe/N/C cathode catalysts for PEFCs. J. Electrochem. Soc. **154**(8), B761–B769 (2007).

6. F. Charreteur, S. Ruggeri, F. Jaouen, J. P. Dodelet, Increasing the activity of Fe/N/C catalysts in PEM fuel cell cathodes using carbon blacks with a high-disordered carbon content. Electrochim. Acta **53**(23), 6881–6889 (2008).

7. C. Domínguez, F. J. Pérez-Alonso, M. A. Salam, S. A. Al-Thabaiti, M. A. Peña, F. J. García-García, L. Barrio, S. Rojas, Repercussion of the carbon matrix for the activity and stability of Fe/N/C electrocatalysts for the oxygen reduction reaction. Appl. Catal. B Environ. **183**, 185–196 (2016).

8. C. Domínguez, F. J. Pérez-Alonso, J. L. Gómez De La Fuente, S. A. Al-Thabaiti, S. N. Basahel, A. O. Alyoubi, A. A. Alshehri, M. A. Peña, S. Rojas, Influence of the electrolyte for the oxygen reduction reaction with Fe/N/C and Fe/N/CNT electrocatalysts. J. Power Sources **271**, 87–96 (2014).

9. J. Li, S. Ghoshal, W. Liang, M. T. Sougrati, F. Jaouen, B. Halevi, S. McKinney, G. McCool, C. Ma, X. Yuan, Z. F. Ma, S. Mukerjee, Q. Jia, Structural and mechanistic basis for the high activity of Fe-N-C catalysts toward oxygen

reduction. Energy Environ. Sci. **9**(7), 2418–2432 (2016).
10. A. Zitolo, V. Goellner, V. Armel, M. T. Sougrati, T. Mineva, L. Stievano, E. Fonda, F. Jaouen, Identification of catalytic sites for oxygen reduction in iron- and nitrogen-doped graphene materials. Nat. Mater. **14**(9), 937–942 (2015).
11. Q. Jia, N. Ramaswamy, U. Tylus, K. Strickland, J. Li, A. Serov, K. Artyushkova, P. Atanassov, J. Anibal, C. Gumeci, S. C. Barton, M. T. Sougrati, F. Jaouen, B. Halevi, S. Mukerjee, Spectroscopic insights into the nature of active sites in iron–nitrogen–carbon electrocatalysts for oxygen reduction in acid. Nano Energy **29**, 65–82 (2016).
12. E. Proietti, F. Jaouen, M. Lefèvre, N. Larouche, J. Tian, J. Herranz, J. P. Dodelet, Iron-based cathode catalyst with enhanced power density in polymer electrolyte membrane fuel cells. Nat. Commun. **2**(1), 416 (2011).
13. B. Nagy, I. Bakos, I. Bertóti, A. Domán, A. Menyhárd, M. Mohai, K. László, Synergism of nitrogen and reduced graphene in the electrocatalytic behavior of resorcinol - Formaldehyde based carbon aerogels. Carbon N. Y. **139**, 872–879 (2018).
14. F. Li, L. Xie, G. Sun, Q. Kong, F. Su, Y. Cao, J. Wei, A. Ahmad, X. Guo, C. M. Chen, Resorcinol-formaldehyde based carbon aerogel: Preparation, structure and applications in energy storage devices. Microporous Mesoporous Mater. **279**, 293–315 (2019).
15. G. Rasines, P. Lavela, C. Macías, M. C. Zafra, J. L. Tirado, C. O. Ania, On the use of carbon black loaded nitrogen-doped carbon aerogel for the electrosorption of sodium chloride from saline water. Electrochim. Acta **170**, 154–163 (2015).
16. G. Rasines, P. Lavela, C. Macías, M. C. Zafra, J. L. Tirado, J. B. Parra, C. O. Ania, N-doped monolithic carbon aerogel electrodes with optimized features for the electrosorption of ions. Carbon N. Y. **83**, 262–274 (2015).
17. H. W. Liang, Z. Y. Wu, L. F. Chen, C. Li, S. H. Yu, Bacterial cellulose derived nitrogen-doped carbon nanofiber aerogel: An efficient metal-free oxygen reduction electrocatalyst for zinc-air battery. Nano Energy **11**, 366–376 (2015).
18. A. Sarapuu, L. Samolberg, K. Kreek, M. Koel, L. Matisen, K. Tammeveski, Cobalt- and iron-containing nitrogen-doped carbon aerogels as non-precious metal catalysts for electrochemical reduction of oxygen. J. Electroanal. Chem. **746**, 9–17 (2015).
19. A. Allahbakhsh, A. R. Bahramian, Self-assembled and pyrolyzed carbon aerogels: An overview of their preparation mechanisms, properties and applications. Nanoscale **7**(34), 14139–14158 (2015).
20. D. Long, J. Zhang, J. Yang, Z. Hu, G. Cheng, X. Liu, R. Zhang, L. Zhan, W. Qiao, L. Ling, Chemical state of nitrogen in carbon aerogels issued from phenol-melamine-formaldehyde gels. Carbon N. Y. **46**(9), 1259–1262 (2008).
21. A. Sarapuu, K. Kreek, K. Kisand, M. Kook, M. Uibu, M. Koel, K. Tammeveski, Electrocatalysis of oxygen reduction by iron-containing nitrogen-doped carbon aerogels in alkaline solution. Electrochim. Acta **230**, 81–88 (2017).
22. S. Liu, C. Deng, L. Yao, H. Zhong, H. Zhang, The key role of metal dopants in nitrogen-doped carbon xerogel for oxygen reduction reaction. J. Power Sources **269**, 225–235 (2014).
23. K. Elumeeva, J. Ren, M. Antonietti, T. P. Fellinger, High Surface Iron/Cobalt-Containing Nitrogen-Doped Carbon Aerogels as Non-Precious Advanced Electrocatalysts for Oxygen Reduction. ChemElectroChem **2**(4), 584–591 (2015).
24. A. A. Gewirth, J. A. Varnell, A. M. Diascro, Nonprecious Metal Catalysts for Oxygen Reduction in Heterogeneous Aqueous Systems. Chem. Rev. **118**(5), 2313–2339 (2018).
25. H. Zhou, S. Xu, H. Su, M. Wang, W. Qiao, L. Ling, D. Long, Facile preparation and ultra-microporous structure of melamine-resorcinol- formaldehyde polymeric microspheres. Chem. Commun. **49**(36), 3763–3765 (2013).
26. B. Nagy, S. Villar-Rodil, J. M. D. Tascón, I. Bakos, K. László, Nitrogen doped mesoporous carbon aerogels and implications for electrocatalytic oxygen reduction reactions. Microporous Mesoporous Mater. **230**, 135–144 (2016).

27. J. Jagiello, J. P. Olivier, Carbon slit pore model incorporating surface energetical heterogeneity and geometrical corrugation. Adsorption **19**(2–4), 777–783 (2013).
28. A. M. Puziy, O. I. Poddubnaya, B. Gawdzik, M. Sobiesiak, Comparison of heterogeneous pore models QSDFT and 2D-NLDFT and computer programs ASiQwin and SAIEUS for calculation of pore size distribution. Adsorption **22**(4–6), 459–464 (2016).
29. P. Veselá, V. Slovák, Monitoring of N-doped organic xerogels pyrolysis by TG-MS. J. Therm. Anal. Calorim. **113**(1), 209–217 (2013).
30. C. Macías, M. Haro, J. B. Parra, G. Rasines, C. O. Ania, Carbon black directed synthesis of ultrahigh mesoporous carbon aerogels. Carbon N. Y. **63**, 487–497 (2013).
31. T. K. Sherwood, E. R. Gilliland, S. W. Ing, Hydrogen Cyanide Synthesis from Its Elements and from Ammonia and Carbon. Ind. Eng. Chem. **52**(7), 601–604 (1960).
32. M. Lefèvre, J. P. Dodelet, Fe-based electrocatalysts made with microporous pristine carbon black supports for the reduction of oxygen in PEM fuel cells. Electrochim. Acta **53**(28), 8269–8276 (2008).
33. F. Jaouen, F. Charreteur, J. P. Dodelet, Fe-based catalysts for oxygen reduction in PEMFCs. J. Electrochem. Soc. **153**(4), A689–A698 (2006).
34. F. Charreteur, F. Jaouen, S. Ruggeri, J. P. Dodelet, Fe/N/C non-precious catalysts for PEM fuel cells: Influence of the structural parameters of pristine commercial carbon blacks on their activity for oxygen reduction. Electrochim. Acta **53**(6), 2925–2938 (2008).
35. D. Zhai, H. Du, B. Li, Y. Zhu, F. Kang, Porous graphitic carbons prepared by combining chemical activation with catalytic graphitization. Carbon N. Y. **49**(2), 725–729 (2011).
36. A. Serov, A. D. Shum, X. Xiao, V. De Andrade, K. Artyushkova, I. V. Zenyuk, P. Atanassov, Nano-structured platinum group metal-free catalysts and their integration in fuel cell electrode architectures. Appl. Catal. B Environ. **237**(August 2017), 1139–1147 (2018).
37. H. R. Byon, J. Suntivich, Y. Shao-Horn, Graphene-based non-noble-metal catalysts for oxygen reduction reaction in acid. Chem. Mater. **23**(15), 3421–3428 (2011).
38. N. Brun, S. A. Wohlgemuth, P. Osiceanu, M. M. Titirici, Original design of nitrogen-doped carbon aerogels from sustainable precursors: Application as metal-free oxygen reduction catalysts. Green Chem. **15**(9), 2514–2524 (2013).
39. K. Artyushkova, A. Serov, S. Rojas-Carbonell, P. Atanassov, Chemistry of Multitudinous Active Sites for Oxygen Reduction Reaction in Transition Metal-Nitrogen-Carbon Electrocatalysts. J. Phys. Chem. C **119**(46), 25917–25928 (2015).
40. D. Guo, R. Shibuya, C. Akiba, S. Saji, T. Kondo, J. Nakamura, Active sites of nitrogen-doped carbon materials for oxygen reduction reaction clarified using model catalysts. Electrochemistry **351**(6271), 361–366 (2016).
41. W. J. Jiang, L. Gu, L. Li, Y. Zhang, X. Zhang, L. J. Zhang, J. Q. Wang, J. S. Hu, Z. Wei, L. J. Wan, Understanding the High Activity of Fe-N-C Electrocatalysts in Oxygen Reduction: $Fe/Fe_3C$ Nanoparticles Boost the Activity of $Fe-N_x$. J. Am. Chem. Soc. **138**(10), 3570–3578 (2016).
42. P. Xu, W. Chen, Q. Wang, T. Zhu, M. Wu, J. Qiao, Z. Chen, J. Zhang, Effects of transition metal precursors (Co, Fe, Cu, Mn, or Ni) on pyrolyzed carbon supported metal-aminopyrine electrocatalysts for oxygen reduction reaction. RSC Adv. **5**(8), 6195–6206 (2015).
43. X. Yang, Y. Wang, G. Zhang, L. Du, L. Yang, M. Markiewicz, J. yeon Choi, R. Chenitz, S. Sun, $SiO_2$-Fe/N/C catalyst with enhanced mass transport in PEM fuel cells. Appl. Catal. B Environ. **264**(June 2019), 118523 (2020).

44. F. Jaouen, J. Herranz, M. Lefévre, J. P. Dodelet, U. I. Kramm, I. Herrmann, P. Bogdanoff, J. Maruyama, T. Nagaoka, A. Garsuch, J. R. Dahn, T. Olson, S. Pylypenko, P. Atanassov, E. A. Ustinov, Cross-laboratory experimental study of non-noble-metal electrocatalysts for the oxygen reduction reaction. ACS Appl. Mater. Interfaces **1**(8), 1623–1639 (2009).
45. Y. Hanzawa, H. Hatori, N. Yoshizawa, Y. Yamada, Structural changes in carbon aerogels with high temperature treatment. J. Carbon Res. Artic. **40**(4), 575–581 (2002).
46. F. Charreteur, F. Jaouen, J. P. Dodelet, Iron porphyrin-based cathode catalysts for PEM fuel cells: Influence of pyrolysis gas on activity and stability. Electrochim. Acta **54**(26), 6622–6630 (2009).